

# Learning with Weak Annotations for Robust Maritime Obstacle Detection

Lojze Žust and Matej Kristan

Faculty of Computer and Information Science, University of Ljubljana, Večna pot 113,  
Ljubljana, 1000, Slovenia.

\*Corresponding author(s). E-mail(s): [lojze.zust@fri.uni-lj.si](mailto:lojze.zust@fri.uni-lj.si);  
Contributing authors: [matej.kristan@fri.uni-lj.si](mailto:matej.kristan@fri.uni-lj.si);

## Abstract

Robust maritime obstacle detection is crucial for safe navigation of autonomous boats and timely collision avoidance. The current state-of-the-art is based on deep segmentation networks trained on large datasets. Per-pixel ground truth labeling of such datasets, however, is labor-intensive and expensive. We propose a new scaffolding learning regime (SLR), that leverages weak annotations consisting of water edge, horizon and obstacle bounding boxes to train segmentation-based obstacle detection networks, and thus reduces the required ground truth labelling effort by twenty-fold. SLR trains an initial model from weak annotations, then alternates between re-estimating the segmentation pseudo labels and improving the network parameters. Experiments show that maritime obstacle segmentation networks trained using SLR on weak labels not only match, but outperform the same networks trained with dense ground truth labels, which is a remarkable result. In addition to increased accuracy, SLR also increases domain generalization and can be used for domain adaptation with a low manual annotation load. The code and pre-trained models are available at <https://github.com/lojzezust/SLR>.

**Keywords:** semantic segmentation, weak supervision, obstacle detection, maritime perception

## 1 Introduction

Autonomous boats have a significant commercial and societal potential in trans-ocean cargo shipping, passenger ferrying, inspection of hazardous areas and environmental control. Their autonomy crucially relies on obstacle detection, which is particularly challenging in maritime domains like coastal waters, marinas, city canals and rivers. The reason is that the appearance of the navigable surface (water) is dynamic, varies with weather and contains object reflections and glitter. Similar holds for the obstacles – these can be static (*e.g.*, shore and piers) or dynamic (*e.g.*, boats,

swimmers, debris, buoys) with a broad range of appearances.

The current state-of-the-art in vision-based maritime obstacle detection (Bovcon et al, 2021) is based on the segmentation of captured images into water, obstacle and sky classes. In contrast to detection-based methods, segmentation methods simultaneously address the detection of static and dynamic obstacles, are more robust to the diverse appearance of obstacle types and directly detect the navigable area (water). However, their performance depends on the availability of large per-pixel segmented training datasets (Bovcon et al, 2019).

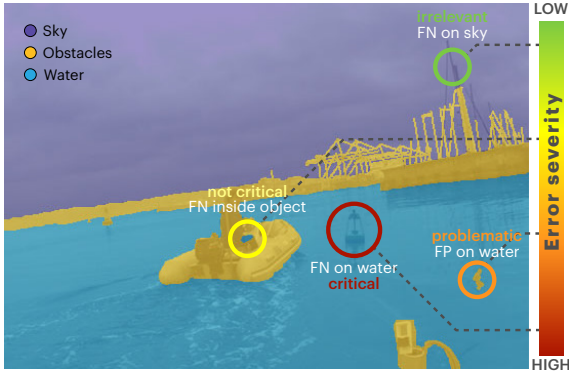


**Fig. 1** Equally large obstacle segmentation errors in different regions have significantly different implications for the downstream task of collision avoidance and boat navigation.

Manual segmentation of training sets is time-consuming, costly and error-prone. For example, manual segmentation of a typical maritime image takes approximately 20 minutes (Bovcon et al, 2019). In a related field of autonomous cars, significant efforts have thus been invested in semi-automatic annotation (Maninis et al, 2018; Zhang et al, 2020b), domain transfer (Vu et al, 2019; Yang and Soatto, 2020), semi-supervised learning (Huo et al, 2021; Mittal et al, 2019) and weak supervision (Li et al, 2018; Wang et al, 2020b) to reduce the required labeling effort. However, annotation requirements may be further reduced by considering the specifics of downstream applications.

We observe that segmentation errors in different semantic regions may have profoundly different consequences for maritime navigation. Figure 1 visualizes several of these cases. Detecting the boundary between water and static obstacles (*i.e.*, the water edge) is crucial for collision prevention, while accurate segmentation of the shore-sky boundary is irrelevant for obstacle avoidance. Similarly, miss-classifying a few pixels on a floating obstacle will not cause a collision, but falsely classifying isolated patches of water pixels as an obstacle will detrimentally affect the control, causing frequent and unnecessary stops. The recent maritime obstacle detection benchmarks (Bovcon et al, 2021) also reflect these navigation-specific segmentation requirements by defining performance evaluation measures, which evaluate the performance in terms of dynamic obstacle detection and water-edge estimation accuracy, while the

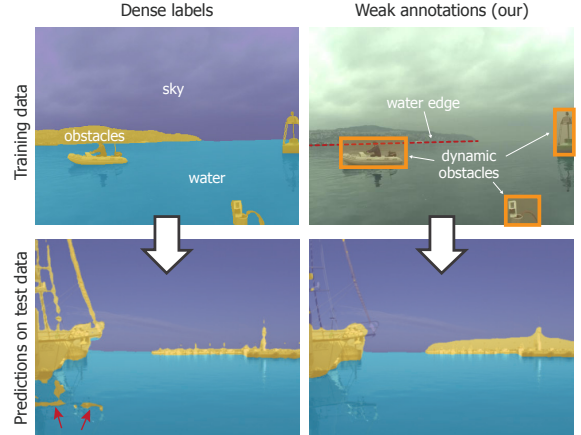


**Fig. 2** The proposed scaffolding learning regime (SLR) trains a network with weak obstacle-oriented annotations (upper right) without hampering the segmentation quality relevant for obstacle detection (bottom).

segmentation accuracy beyond the water boundary is ignored.

Taking into account the aforementioned requirements of the maritime obstacle detection task, we propose a new scaffolding learning regime (SLR), which is our main contribution. SLR avoids the need for densely labeled ground truth for training maritime obstacle detection networks and instead relies only on weak obstacle-oriented annotations (Figure 2) consisting of water-edge polylines, bounding boxes denoting dynamic obstacles and the horizon location estimated from the on-board inertial measurement unit (IMU) data. At a high level, SLR works by EM-like steps, alternating between estimating the unknown segmentation labels and improving the network parameters. First, by considering the domain constraints, we can construct partial segmentation labels (*i.e.*, not all pixels are labeled) from weak annotations. A segmentation network is then trained on the partial labels to learn domain-specific feature extraction. During this initialization step, we also use additional bounding-box-based training objectives to learn the segmentation of foreground dynamic obstacles.

In turn, the trained network is used to estimate the labels in the unknown regions of the image. While the predictions of such a network cannot be expected to reach the desired robustness due to the complex interplay of multiple training objectives, the encoder must learn powerful domain-specific features to satisfy all the

objectives. We thus employ a feature clustering approach, to infer the most likely labels for unlabeled pixels in the partial segmentation labels. Finally, the network is fine-tuned on the newly estimated pseudo labels.

Extensive evaluation on maritime obstacle detection by segmentation (Bovcon et al, 2021) shows that models trained using SLR outperform models classically trained on full dense annotations, which is a remarkable result. In fact, the new training regime increases robustness to false-positive detections and improves the generalization capabilities of the trained networks, while reducing the required ground truth annotation time by orders of magnitude. To the best of our knowledge, this is the first method for training obstacle detection from weak annotations in the marine domain which surpasses fully supervised training from dense labels.

Preliminary results of our approach were presented in a conference paper (Žust and Kristan, 2022). This paper goes beyond the preliminary work in several ways: we introduce an additional auxiliary object loss and re-formulate the training method, which leads to a substantial performance improvement. The experimental analysis is also significantly extended with a cross-domain generalization analysis, an annotation efficiency study including a comparison with a recent state-of-the-art annotation-reduction approach (*i.e.*, semi-supervised learning), experiments and discussion with soft labels, as well as qualitative analysis on a wide range of maritime images.

## 2 Related work

In the following, we overview the related work in maritime obstacle detection (Section 2.1) and label-efficient training for deep segmentation models (Section 2.2).

### 2.1 Maritime obstacle detection

Early approaches for obstacle detection in the marine domain include handcrafted methods such as background subtraction (Prasad et al, 2019), stereo reconstruction (Wang and Wei, 2013) and statistical semantic segmentation methods with color and texture features (Kristan et al, 2016; Bai et al, 2016). However, due to the challenging dynamics of the water surface, these methods

struggle in challenging scenes and tend to produce a large amount of FP detections.

For this reason, similarly to the autonomous ground vehicles (AGV), the perception in marine robotics has shifted towards deep learning methods in recent years, enabling the learning of rich visual features specialized for the target task. Early works (Lee et al, 2018; Moosbauer et al, 2019; Yang et al, 2019) were based on the direct application of classical deep general object detection methods (Ren et al, 2017; Liu et al, 2020) or their specializations to ship detection tasks (Ma et al, 2020). Unfortunately, these methods only detect obstacles that can be pre-trained and are in form of compact well-defined objects, while they are unable to address both dynamic and static obstacles such as piers, shorelines and floating fences. Furthermore, the wide variety of obstacle appearances, which is specific to often poorly structured maritime domain, prohibits training of the object-category-specific detectors used in these works.

To address these limitations, several works investigated deep-learning-based semantic segmentation as a possible alternative, posing the problem of obstacle detection as anomaly segmentation, where all obstacles (static and dynamic) are assigned to a single *obstacle* class. However, due to the specifics of the maritime domain (dynamics of the water surface, reflections), applying well-established semantic segmentation models from the AGV domain (Chen et al, 2017; Yu et al, 2021) to the maritime domain lacks the desired robustness (Bovcon et al, 2019; Cane and Ferryman, 2019).

For this reason, several networks designed specifically for the maritime domain have been recently proposed (Kim et al, 2019; Steccanella et al, 2020; Bovcon and Kristan, 2021; Qiao et al, 2022). Networks by Steccanella et al (2020) and Yao et al (2021) are based on the U-net architecture (Ronneberger et al, 2015) and utilize various regularization and data augmentation techniques to increase their robustness. Recently, Bovcon and Kristan (2021) introduced a novel architecture WaSR, which harnesses additional information from the on-board IMU measurements to estimate the horizon location prior, which is fused with the image features in the network decoder. Additionally, a water-separation loss is proposed to encourage learning a better separation of water

and obstacle features in the model encoder. The approach greatly reduces the sensitivity of the network to changes in the water appearance and is the current state-of-the-art on the USV obstacle detection benchmark MODS (Bovcon et al, 2021). A maritime domain panoptic segmentation approach has also been proposed (Qiao et al, 2022), enabling the distinction between obstacle instances, but has only been applied to a limited task of ship detection (Prasad et al, 2017) from mostly static on-shore sequences.

As shown by Bovcon et al (2021), current state-of-the-art approaches still lack the desired robustness, especially within the most critical 15m radius around the boat (*i.e.*, the danger zone) and struggle with domain-specific artefacts such as waves, object reflections and sun glitter. Further development of the field is also limited by the low availability of per-pixel annotated datasets (Bovcon et al, 2019; Cheng et al, 2021; Qiao et al, 2022), the annotation of which is costly and error-prone. Our work partly addresses this issue by proposing a method for learning maritime semantic segmentation networks from weak labels, thereby avoiding the need for per-pixel labeling and significantly reducing the labelling effort. In addition, the method improves the robustness of the learned networks by considering the downstream task during training.

## 2.2 Reducing the annotation effort

The development of deep segmentation models is hampered by their reliance on large amounts of painstakingly labeled training data. Recent annotation-efficient training methods thus aim to achieve a better trade-off between model performance and annotation effort. Semi-supervised methods (Hung et al, 2019; Mittal et al, 2019; Huo et al, 2021) aim to harness additional unlabeled images to improve segmentation accuracy. Theoretically, this could also reduce the required labeling effort by reducing the amount of required labeled images. However, as the annotation effort is mainly reduced by labeling fewer images, such methods are more sensitive to labeling errors and can only capture a limited visual variation of open-ended classes such as obstacles.

Alternatively, weakly-supervised methods (Chan et al, 2021) reduce the annotation effort by using weaker forms of labels. Approaches

like expectation maximization (Papandreou et al, 2015), multiple instance learning (Durand et al, 2017) and self-supervised learning (Ahn and Kwak, 2018; Wang et al, 2020c,a; Pan et al, 2022) have been considered to learn semantic segmentation of objects from image-level labels. These approaches can infer the information about class appearances from the differences between images containing and images not containing objects of a certain class. As such they are well-suited for natural images, with a relatively small number of objects per image and a large vocabulary of classes, where image-level labels are informative to the content of the image. However, for general scene parsing required for obstacle detection in autonomous vehicles and boats, where many objects are present in the scene at once, often including multiple instances of the same class (*i.e.*, obstacles), such approaches do not perform well (Wang et al, 2020b). This is especially problematic in domains with a small number of classes such as anomaly segmentation in the marine domain (3 classes), where all classes are present in most of the scenes and thus image-level labels provide almost no discriminative information.

Other approaches like scribbles (Vernaza and Chandraker, 2017; Zhang et al, 2020a) and point annotations (Maninis et al, 2018; Akiva et al, 2020) have also been considered for this task. These provide the information for the most representative pixels of an object but fail to capture the extent or boundaries of objects, which are very important for boat navigation. Bounding boxes are much more suitable for this task, as they provide information both about the location of an object as well as weak constraints on its boundary. Due to these informative cues, ease of annotation and their ubiquitous presence, bounding boxes have been extensively studied as weak constraints in many segmentation tasks, including semantic segmentation (Dai et al, 2015; Kulharia et al, 2020), instance segmentation (Hsu et al, 2019; Tian et al, 2021) and video object segmentation (Zhao et al, 2021). However, these approaches mainly focus on the segmentation of well-defined foreground objects (*e.g.*, dynamic obstacles), but are not designed to learn boundaries between background classes (*e.g.*, static obstacles), which are required for general scene parsing and obstacle detection in AGVs or USVs.



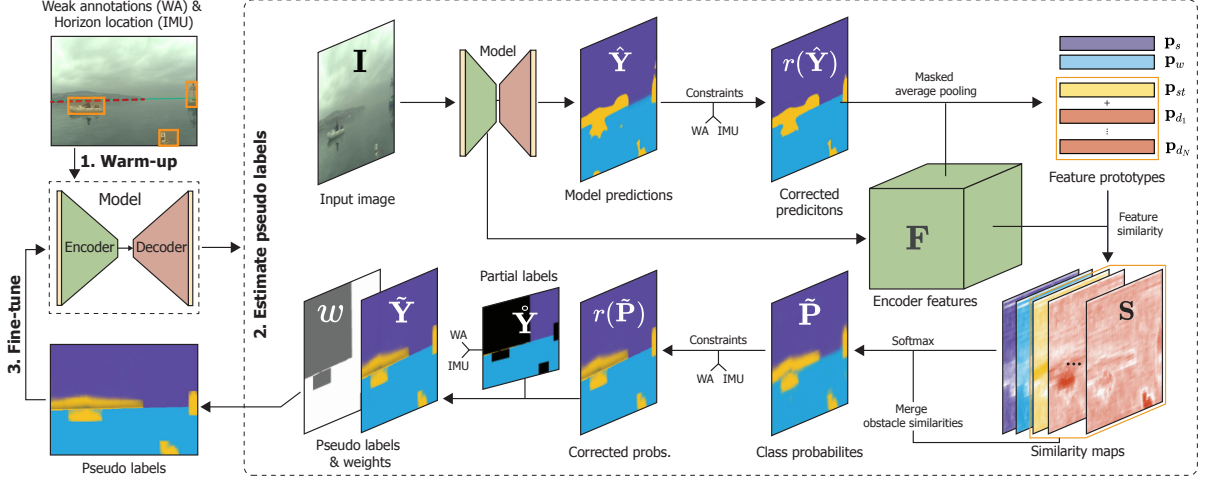


**Fig. 3** The proposed scaffolding approach SLR is comprised of three steps. (1) The model is warmed-up using object-wise and global objectives derived from weak annotations and IMU. (2) The learned encoder features and model predictions are used to estimate the pseudo labels. (3) The network is fine-tuned with the estimated pseudo labels.

Instead, general scene parsing must account both for the segmentation of foreground objects as well as background classes, thus a combination of different weak-annotation types may be more appropriate. The method introduced by Li et al (2018) uses bounding boxes to supervise the learning of foreground classes, while image-level labels are used to supervise the learning of the background class, which is possible due to a large vocabulary of background classes. This, however, is not the case in the maritime domain, where there are only three classes. Furthermore, from the perspective of maritime obstacle detection, a single aspect of background segmentation is the most important – the boundaries of the water surface. Instead of image-level labels we thus propose the use of water-edge annotations for supervising the background segmentation, thus focusing the annotation effort on this crucial information, at a comparable effort to less focused image-level labels.

### 3 Learning segmentation by scaffolding

We now introduce the new maritime segmentation networks learning approach, which we call the scaffolding learning regime (SLR). SLR gradually improves the trained model by iterating between improving the network parameters using per-pixel (pseudo-) labels and re-estimating the

pseudo labels by the learned network. This process is composed of three steps shown in Figure 3. In the first step (Section 3.1) the network is trained using 1) partial labels, which are constructed from weak annotations and domain constraints and 2) additional weak objectives for learning the segmentation of dynamic obstacles. In the second step (Section 3.2), the learned network is used to estimate the labels of unlabeled regions in partial labels. Finally (Section 3.3), the network is fine-tuned using the estimated pseudo labels. These three steps are detailed in the following.

#### 3.1 Feature warm-up

The purpose of the feature warm-up step is to learn domain-specific encoder features and initial segmentation predictions. This is achieved by weakly-supervised training. Specifically, combining domain knowledge and weak annotations, we can label certain regions of an input image  $\mathbf{I} \in \mathbb{R}^{W \times H \times 3}$  with high confidence, while others remain unlabeled, producing partial labels  $\hat{\mathbf{Y}} \in [0, 1]^{W \times H \times 3}$  (Section 3.1.1), which can be used to supervise the model training (Section 3.1.2).

##### 3.1.1 Partial labels from weak annotations

To generate per-pixel partial labels  $\hat{\mathbf{Y}} = (\hat{\mathbf{Y}}_w, \hat{\mathbf{Y}}_s, \hat{\mathbf{Y}}_o)$  for the water, sky and obstacle class

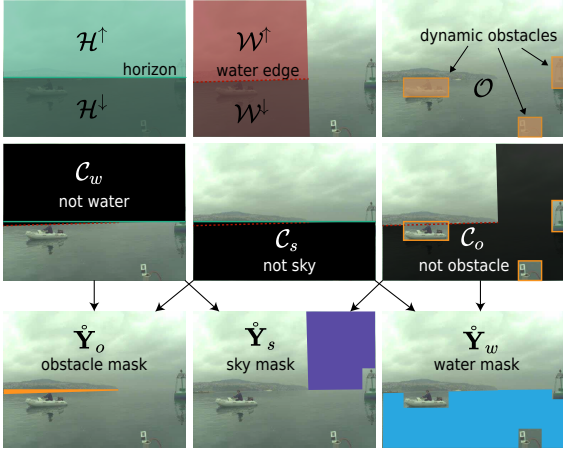


**Fig. 4** The weak annotations (top) form domain-specific constraints (middle), which restrict the possible per-pixel labels and generate the initial partial labels (bottom).

respectively, we introduce domain-specific constraints extrapolated from weak annotations and horizon location estimated from the IMU (following [Bovcon and Kristan \(2021\)](#)), as shown in Figure 4. The estimated horizon splits the image into two sets: regions above it ( $\mathcal{H}^\uparrow$ ) and regions below it ( $\mathcal{H}^\downarrow$ ). Similarly, water-edge annotations define sets  $\mathcal{W}^\uparrow$  and  $\mathcal{W}^\downarrow$  for regions above and below, respectively, and bounding boxes define the set  $\mathcal{O}$  of rectangular regions tightly containing dynamic obstacles.

Using this notation, we define class-restricted regions  $\mathcal{C}_c$ , in which the class  $c$  cannot appear. Namely, water pixels cannot appear above the horizon or water edge ( $\mathcal{C}_w = \mathcal{H}^\uparrow \cup \mathcal{W}^\uparrow$ ), sky pixels cannot appear below the horizon or water edge ( $\mathcal{C}_s = \mathcal{H}^\downarrow \cup \mathcal{W}^\downarrow$ ) and obstacle pixels cannot appear outside object bounding boxes, except above the water edge ( $\mathcal{C}_o = \mathcal{O}^C \setminus \mathcal{W}^\uparrow$ ). We can thus set the probability for class  $c$  of a pixel  $i$  to 0 inside the respective restricted area. In certain regions, these restrictions lead to unambiguous labels with a single class remaining. In general, the probability of a class  $c$  label at pixel location  $i$  is defined as

$$\hat{\mathbf{Y}}_c^i = \begin{cases} 1 & \text{if } i \notin \mathcal{C}_c \wedge i \in \bigcap_{k \neq c} \mathcal{C}_k, \\ 0 & \text{otherwise.} \end{cases} \quad (1)$$

To account for the missing unique labels at some pixels, we introduce per-pixel training weights  $w_i$ . In particular, the weights are set to  $w_i = 1$  at pixels with unambiguous labels and to

$w_i = 0$  elsewhere. This means that the latter pixels are effectively ignored in training.

From the water-edge annotations, we can also infer that a pixel  $i$ , located immediately above the water edge, must belong to the obstacle class ( $\hat{\mathbf{Y}}_o^i = 1$ ) by definition. However, since the height of the static obstacle is unknown, we employ a heuristic approach and only label a pixel as an obstacle if its distance  $d_i$  from the water edge is below a threshold  $\theta$ , *i.e.*,

$$\hat{\mathbf{Y}}_o^{i \in \mathcal{W}^\uparrow} = \begin{cases} 1 & \text{if } d_i < \theta, \\ 0 & \text{otherwise} \end{cases} \quad (2)$$

We furthermore adjust its weight to reflect the increase of label uncertainty with distance, *i.e.*,  $w_i = \exp(-\alpha d_i)$ , where  $\alpha = -\ln(\omega_{\min})/\theta$  is defined such that all weights lower than a small value  $\omega_{\min}$  are set to zero.

### 3.1.2 Training

The network is trained with a weighted focal loss ([Lin et al, 2020](#))  $\mathcal{L}_{\text{foc}}$  on the partial labels  $\hat{\mathbf{Y}}$  and their corresponding weights  $w_i$ . However, further training signals can be derived for the unlabelled regions corresponding to the dynamic obstacles.

In particular, we use several loss functions inspired by instance segmentation literature ([Tian et al, 2021](#); [Kulharia et al, 2020](#)). We leverage the bounding box annotations with a projection loss  $\mathcal{L}_{\text{proj}}$  ([Tian et al, 2021](#)). The projection loss provides a weak constraint on the segmentation of an obstacle, forcing the horizontal and vertical projection of the segmentation mask to match the edges of the bounding box. Further regularization is applied by using a pairwise loss  $\mathcal{L}_{\text{pair}}$  ([Tian et al, 2021](#)). This loss encourages equal labels on visually similar neighboring pixels. We adapt the pairwise loss term to a multiclass setting and apply it over the entire image, so it supervises both dynamic and static obstacle segmentation.

Finally, we estimate a prior for the segmentation mask for each dynamic obstacle using a pre-trained class-agnostic deep grab-cut segmentation network ([Yan et al, 2021](#)). In turn, a focal loss between the predicted object segmentation and the estimated prior segmentation  $\mathcal{L}_{\text{aux}}$  is used as an auxiliary source of obstacle segmentation supervision.

The final loss is thus composed of global and dynamic obstacle losses:

$$\mathcal{L}_{\text{wrm}} = \mathcal{L}_{\text{foc}}(\hat{\mathbf{Y}}; w) + \mathcal{L}_{\text{pair}} + \sum_{n=1:N} (\mathcal{L}_{\text{proj}}^{(n)} + \mathcal{L}_{\text{aux}}^{(n)}), \quad (3)$$

where  $N$  is the number of annotated dynamic obstacles.

### 3.2 Estimating pseudo labels from features

The model learned in the warm-up phase (Section 3.1) cannot be expected to produce robust predictions due to a complex combination of training objectives used during training. However, to address all training objectives simultaneously, the encoder must learn strong domain-specific features. We thus estimate the labels of unlabeled regions of the partial labels  $\hat{\mathbf{Y}}$  based on feature clustering in the learned feature space producing dense pseudo labels  $\tilde{\mathbf{Y}}$ . This process is based on the assumption that pixels corresponding to the same semantic class cluster together in the learned feature space.

We first correct the model predictions with constraints derived from weak annotations. Let  $\hat{\mathbf{Y}} = (\hat{\mathbf{Y}}_w, \hat{\mathbf{Y}}_s, \hat{\mathbf{Y}}_o) \in [0, 1]^{W \times H \times 3}$  be the model predictions (probabilities) for the water, sky and obstacle class and  $\mathbf{F} \in \mathcal{R}^{W \times H \times C}$  be the feature maps produced by the encoder for an input image  $\mathbf{I}$ . We define  $r(\cdot)$  as a function that corrects (*i.e.*, constrains) the labels according to the domain constraints – the probability for class  $c$  is set to 0 in restricted locations  $i$  as in Section 3.1.1, *i.e.*,  $r(\hat{\mathbf{Y}}_c^i) = 0; \forall i \in \mathcal{C}$ .

From the constrained predictions  $\mathbf{R} = r(\hat{\mathbf{Y}})$ , class prototypes are constructed. A class prototype  $\mathbf{p}_c$  is a single feature vector describing the class  $c$  and is computed as a masked average pooling over the features

$$\mathbf{p}_c = \frac{\sum_{i \in \mathbf{I}} \mathbf{R}_c^i \mathbf{F}^i}{\sum_{i \in \mathbf{I}} \mathbf{R}_c^i}, \quad (4)$$

where  $\mathbf{F}^i$  and  $\mathbf{R}_c^i$  denote the features and constrained probabilities of class  $c$  at an image location  $i$ . Because dynamic obstacle appearance might vary greatly across instances, we construct separate prototypes  $\mathbf{p}_{d_1}, \dots, \mathbf{p}_{d_N}$  for individual dynamic obstacles in the image (from obstacle

features within the corresponding bounding box) and a separate single prototype  $\mathbf{p}_{st}$  for all the remaining static obstacles. Two prototypes,  $\mathbf{p}_w$  and  $\mathbf{p}_s$ , are extracted for the water and sky class respectively.

The distances between a feature vector and the extracted prototypes are used to determine the class probabilities of a pixel. First, we compute the feature similarity with the constructed prototypes at every image location to produce similarity maps  $\mathbf{S}$  for each of the prototypes. The similarity map  $\mathbf{S}_c$  for class  $c$  at image location  $i$  is computed by cosine similarity

$$\mathbf{S}_c^i = \frac{\mathbf{F}^i \cdot \mathbf{p}_c}{\|\mathbf{F}^i\| \|\mathbf{p}_c\|}. \quad (5)$$

Due to introducing multiple prototypes for the obstacle class, we obtain multiple obstacle similarity maps, which need to be merged into a single obstacle similarity map  $\mathbf{S}_o$  as follows: similarity maps for each of the dynamic obstacles ( $\mathbf{S}_{d_1}, \dots, \mathbf{S}_{d_N}$ ) are applied inside their respective obstacle bounding boxes, and the static obstacle similarity map  $\mathbf{S}_{st}$  is used elsewhere. In areas where annotations of multiple dynamic obstacles overlap, the maximum of their respective similarity values is used.

We can then apply a softmax over the class similarities to obtain the class probability distribution for each location  $i$ , *i.e.*,

$$\tilde{\mathbf{P}}_c^i = \frac{\exp(\beta \mathbf{S}_c^i)}{\sum_k \exp(\beta \mathbf{S}_k^i)}, \quad (6)$$

where  $\mathbf{S} = (\mathbf{S}_w, \mathbf{S}_s, \mathbf{S}_o)$  are the class similarity maps and  $\beta$  is a scaling hyperparameter. The resulting probabilities are corrected using  $r(\cdot)$  to agree with the weak annotation constraints.

Finally, the obtained per-class probabilities are used as the most likely estimates of the missing labels in the unconstrained areas, yielding soft pseudo-labels  $\tilde{\mathbf{Y}}$ , *i.e.*,

$$\tilde{\mathbf{Y}}^i = \begin{cases} r(\tilde{\mathbf{P}}^i) & \text{if } i \text{ not labeled in } \hat{\mathbf{Y}}, \\ \hat{\mathbf{Y}}^i & \text{otherwise.} \end{cases} \quad (7)$$

The corresponding weights for these regions are set to a constant weight  $w_i = \omega_R < 1$  to reflect that these estimated labels are less certain

than the partial labels derived directly from weak annotations.

### 3.3 Fine-tuning with dense pseudo labels

In the final step, the model trained in the warm-up stage is fine-tuned by optimizing a weighted focal loss between the predicted labels and the re-estimated dense pseudo labels and a global pairwise loss, *i.e.*,

$$\mathcal{L}_{\text{finetune}} = \mathcal{L}_{\text{foc}}(\tilde{\mathbf{Y}}) + \mathcal{L}_{\text{pair}}. \quad (8)$$

## 4 Results

A battery of experiments was conducted to probe the learning capabilities of SLR in the context of maritime obstacle detection. In all experiments, the focal loss parameter is set to  $\gamma = 2$  and the remaining SLR hyper-parameters to  $\theta = 11$ ,  $\omega_{\min} = 0.005$ ,  $\beta = 20$  and  $\omega_R = 0.5$ . The number of training epochs in the warm-up and fine-tuning phases is 25 and 50, respectively. Unless stated otherwise, we stop the training after a single SLR iteration (*i.e.*, pseudo-label estimation and model fine-tuning). SLR is demonstrated on the state-of-the-art maritime obstacle detection network WaSR (Bovcon and Kristan, 2021), which employs a ResNet-101 backbone as the encoder. In the warm-up phase, the encoder is initialized from pre-trained weights on Imagenet, while the remaining network weights are initialized randomly. Features from the penultimate (third) encoder residual block are used in the pseudo-label estimation phase after warm-up (Section 3.2). The water separation loss with weight  $\lambda_{\text{ws}} = 0.01$  from WaSR is added to the losses in the fine-tuning step (Section 3.3). Following (Bovcon et al, 2019), all networks are trained with RMSProp optimizer with momentum 0.9, initial learning rate  $10^{-6}$ , standard polynomial reduction decay 0.9 and a batch size of 12. Random image augmentations including color transformations, horizontal flipping, scaling and rotation are applied to training images.

### 4.1 Evaluation protocol

The standard obstacle detection evaluation protocol from the MODS (Bovcon et al, 2021)

benchmark is used. The networks are trained on MaSTr1325 (Bovcon et al, 2019), which contains 1325 diverse, fully per-pixel labeled images captured from unmanned surface vehicles (USV). To evaluate SLR, we additionally annotated the images with water edges and object bounding boxes. The models are evaluated on the test dataset from MODS, which contains approximately 100 sequences annotated by bounding boxes and water edges, using the detection-oriented evaluation protocol (Bovcon et al, 2021). Static obstacle detection is evaluated by water-edge detection robustness ( $\mu_R$ ), which measures the proportion of the water-edge boundary that has been correctly identified (*i.e.*, the boundary is detected within a set threshold distance). Dynamic obstacle detection is evaluated by precision (Pr), recall (Re) and F1 measure. It is evaluated over the entire navigable surface and separately within a 15m *danger zone* from the USV ( $F1_D$ ), where the obstacle detection performance is most critical for immediate collision prevention.

### 4.2 Comparison with full supervision

SLR was evaluated by training two of the top models from the recent MODS (Bovcon et al, 2021) benchmark, using the weak annotations from MaSTr1325 (Bovcon et al, 2019) and evaluating on the MODS test set. In addition, we trained several top-performing models from the same benchmark (RefineNet (Lin et al, 2017), DeepLabV3 (Chen et al, 2018), BiSeNet (Yu et al, 2018) and our re-implementation of WaSR (Bovcon and Kristan, 2021)) using the dense labels to form a strong baseline. In the following  $(\cdot)_{\text{SLR}}$  denotes the networks trained with SLR.

Results in Table 1 show that, remarkably, both  $\text{WaSR}_{\text{SLR}}$  and  $\text{DeepLabV3}_{\text{SLR}}$  *outperform* their classically-trained counterparts DeepLabV3 and WaSR, despite using considerably simpler weak annotations. DeepLabV3<sub>SLR</sub> outperforms its counterpart by 5.8 and 59.0 percentage points overall and inside the danger zone, respectively. In the case of WaSR, SLR boosts performance by 1.4 (overall) and 5.1 (danger zone) percentage points and sets a new state-of-the-art on the MODS benchmark. We observe that SLR consistently decreases false-positive detections and

**Table 1** Comparison of methods trained with weak annotations using the proposed SLR training (denoted by  $(\cdot)_{\text{SLR}}$ ) and state-of-the-art methods trained classically with dense ground truth labels on the MODS benchmark (Bovcon et al, 2021). Performance is reported in terms of F1 score, precision (Pr), recall (Re) for dynamic obstacle detection and water-edge detection robustness ( $\mu_R$ ).

	$\mu_R$	Overall			Danger zone (<15m)		
		Pr	Re	F1	Pr	Re	F1
RefineNet	97.3	89.0	93.0	91.0	45.1	98.1	61.8
DeepLabV3	96.8	80.1	92.7	86.0	18.6	<b>98.4</b>	31.3
BiSeNet	97.4	90.5	89.9	90.2	53.7	97.0	69.1
WaSR	<b>97.5</b>	95.4	91.7	93.5	82.3	96.1	88.6
DeepLabV3 <sub>SLR</sub>	97.1	94.3	89.4	91.8 (+5.8)	85.5	95.5	90.3 (+59.0)
WaSR <sub>SLR</sub>	97.3	<b>96.7</b>	<b>93.1</b>	<b>94.9</b> (+1.4)	<b>91.5</b>	96.0	<b>93.7</b> (+5.1)

**Table 2** Segmentation accuracy (IoU) of fully-supervised WaSR and WaSR<sub>SLR</sub> for the water, sky and obstacles class, summarized by the mean over classes.

	$\text{IoU}_w$	$\text{IoU}_s$	$\text{IoU}_o$	mIoU
WaSR	<b>99.7</b>	<b>99.8</b>	<b>98.1</b>	<b>99.2</b>
WaSR <sub>SLR</sub>	99.4	99.4	95.0	98.0

increases precision while preserving a high recall (qualitative results in Section 4.9). We speculate that this might be due to detection-based training objectives in SLR, which better reflect the downstream task requirements compared to the standard pixel-based segmentation losses.

### 4.3 Segmentation quality

Since the test set annotations in MODS (Bovcon et al, 2021) do not enable segmentation accuracy analysis, we split the MaStr1325 dataset into training (70%) and test (30%) sets. The standard WaSR and WaSR<sub>SLR</sub> are trained on thus obtained training set and evaluated in terms of IoU on the segmentation ground truth of the test set.

Results in Table 2 show that the WaSR<sub>SLR</sub> segmentation accuracy closely matches that of WaSR with merely a 1.2 decrease in mIoU. This decrease can be attributed to slightly over-segmented objects, missed details and thin structures in the sky, which are labeled as obstacles, but are not important from the obstacle detection perspective (Figure 5).

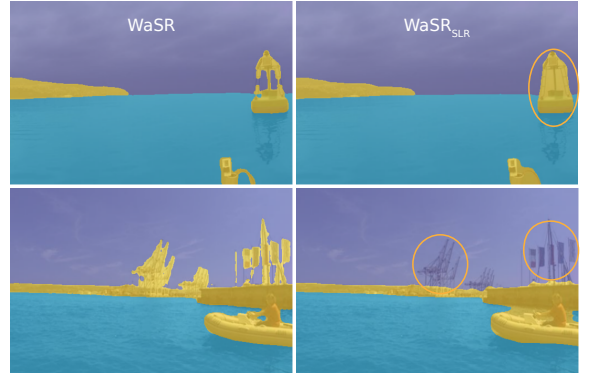


**Fig. 5** Segmentation obtained by WaSR trained with segmentation ground truth (left) and SLR (right). SLR sacrifices segmentation accuracy in regions irrelevant for obstacle detection performance (denoted with yellow circles).

### 4.4 Comparison with semi-supervised learning

SLR can be considered a weakly-supervised learning method, in which the segmentation supervision comes from weak obstacle-oriented annotations. Semi-supervised methods, on the other hand, use a small set of fully-labeled images and a larger set of unlabeled images in training. In both cases, the aim is to reduce the required annotation effort. We thus compare SLR with the recent semi-supervised state-of-the-art method ATSO (Huo et al, 2021) in terms of annotation efficiency. Table 3 compares the two methods and the classical fully-supervised training scheme with varying percentages of the images in the training set.



**Table 3** Annotation efficiency of methods (percentage % of labelled images, and labeling effort  $t$  relative to SLR) in terms of obstacle detection performance on MODS (F1 and  $F1_D$ ) and segmentation on the MaSTr1325 validation set ( $mIoU_{val}$ ).

	%	$t$	$mIoU_{val}$	F1	$F1_D$
WaSR	5	1×	96.3	83.8	69.5
	10	2×	98.4	87.3	78.7
	100	20×	<b>99.8</b>	93.5	88.6
WaSR <sub>ATSO</sub>	5	1×	97.6	90.1	87.5
	10	2×	98.6	91.4	87.0
WaSR <sub>SLR</sub>	100	1×	98.6	<b>94.9</b>	<b>93.7</b>

According to (Bovcon et al, 2019), manual segmentation of a MaSTr1325 image takes approximately 20 minutes. Since weak annotations take 1 min per image, we can estimate that annotation of all images with weak annotations is approximately 5% of the effort required to manually segment all images. We thus first analyse WaSR performance when trained with only 5% of all fully-segmented images (selected at random). Compared to using all training images, the performance in terms of the F1 detection measure substantially drops by almost 10 percentage points overall and 19.1 percentage points within the danger zone. Applying the semi-supervised approach ATSO with 5% of annotated (and 95% non-annotated) training images, significantly improves the performance, particularly within the danger zone (by 18 percentage points). Nevertheless, SLR by far outperforms both fully-supervised and ATSO and achieves a nearly 5 percentage points overall and an over 6 percentage points improvement within the danger zone over ATSO. Even when increasing the annotation effort to 2× that of used with SLR by using 10% of annotations, ATSO still falls short by over 3 percentage points overall and almost 7 percentage points within the danger zone. The results indicate, that SLR and the obstacle-oriented reduction of labels to weak annotations are much more efficient than the general reduction of decreasing the number of labeled images.

For reference, we also evaluate the segmentation performance of the validation set of MaSTr1325. Fully supervised training using all images with ground truth segmentation labels achieves the best  $mIoU$ . Reducing the training

**Table 4** Domain generalization performance on the SMD benchmark (Prasad et al, 2017). Models are trained on MaSTr1325 and bottom two are additionally fine-tuned on the SMD training set.

	Pr	Re	F1
WaSR	87.3	67.0	75.8
WaSR <sub>SLR</sub>	<b>92.8</b>	71.7	80.9 (+5.1)
WaSR <sub>FDA</sub> <sup>ft</sup>	86.9	41.5	56.2 (-19.6)
WaSR <sub>SLR</sub> <sup>ft</sup>	85.6	<b>90.2</b>	<b>90.7</b> (+14.9)

images to match the annotation effort of SLR, results in 3.5 drop in  $mIoU$ . This drop is slightly smaller when using ATSO (2.2 points) and smaller still when using SLR (1.2 points). Segmentation accuracy of ATSO matches that of SLR only when using twice as much manual annotation effort. These results suggest that SLR could potentially be also useful as a method for segmentation ground truth acquisition at a very low manual annotation effort.

#### 4.5 Cross-domain generalization

MaSTr1325 (Bovcon et al, 2019) and MODS (Bovcon et al, 2021) both contain images acquired from the perspective of a small USV. To explore the cross-domain generalization advantages of SLR, we thus perform several experiments by evaluating on the Singapore Marine Dataset (SMD) (Prasad et al, 2017). This dataset presents a different domain than the MaSTr training set and contains video sequences mostly acquired from on-shore vantage points. The objects are annotated with weak annotations, and we use the horizon annotations and the training/test split from (Bovcon and Kristan, 2021).

In the first experiment, we evaluate WaSR trained on MaSTr1325 and test it on the SMD test set. Table 4 shows that SLR outperforms training on segmentation ground truth by 5.1 percentage points, which indicates that better generalization capabilities are obtained purely from the proposed training regime.

We next consider the performance in the context of domain adaptation with MaSTr1325 and SMD training sets used in training and SMD test set for evaluation. We compare SLR with the recent state-of-the-art domain adaptation method FDA (Yang and Soatto, 2020). WaSR trained with FDA performs worse (19 percentage points drop)

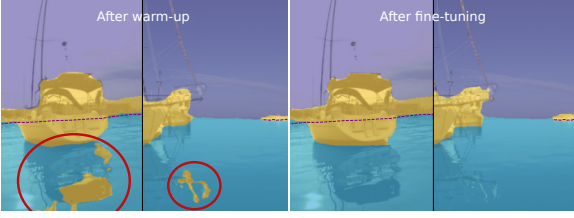


**Fig. 6** The network predicts false positives on, e.g., reflections after warm-up phase (left), while performance improves substantially with fine-tuning on re-estimated labels (right).

than WaSR trained only on the MaStr1325 segmentation ground truth. However, using SLR to fine-tune the model on SMD training set outperforms the latter by nearly 15 percentage points. This implies that SLR bears a strong potential in domain generalization as well as domain adaptation problems.

#### 4.6 Ablation study

To expose the contributions of individual components of SLR, a series of experiments with different components turned off was carried out. Results of training on MaStr1325 and testing on MODS are reported in Table 6.

The most basic model that uses only the feature warm-up step (Section 3.1) without fine-tuning and without the static obstacle labels above the water edge (Section 3.1.1) results in a 7.2 and 38.8 percentage points drop overall and within danger zone, respectively, compared to the full SLR. Detailed inspection showed that this is mainly due to an increased number of false-positive detections (see Figure 6). Adding the static obstacle labels in the warm-up step considerably improves the performance of the basic model (by 16.1 percentage points within the danger zone). A further boost of 13.9 percentage points within the danger zone is obtained by enabling the fine-tuning step (Section 3.3).

Applying the label constraints ( $r(\cdot)$ ) from Section 3.2 leads to further 4.4 percentage points improvement within the danger zone, while only enabling the feature-based re-estimation of pseudo labels (Section 3.2) leads to a 4.8 percentage points improvement. Combining both label constraints and label re-estimation results in 3.7 (overall) and 6.5 (danger zone) percentage points

**Table 5** MODS detection (F1 /  $F1_D$ ) and water-edge estimation robustness ( $\mu_R$ ) with respect to the number of SLR pseudo-label estimation and fine-tuning iterations ( $N_{it}$ ).

$N_{it}$	$\mu_R$	F1	$F1_D$
0	<b>97.8</b>	87.4	57.5
1	97.3	<b>94.9</b>	<b>93.7</b>
2	97.0	94.2	92.1
3	96.9	94.3	93.2
4	97.0	93.7	92.5
5	96.9	93.7	92.4

improvements over the model without the predictions refinement step. Finally, using the auxiliary per-object segmentation loss ( $\mathcal{L}_{aux}$ ) during warm-up, further improves the performance by 0.7 and 2.3 points respectively. The mIoU (Table 6) between the predicted segmentation masks and the ground truth labels on the validation set, shows that each SLR module consistently contributes to learning the unknown underlying segmentation.

#### 4.7 Influence of SLR iterations

The number of SLR iterations composed of the pseudo-labels estimation (Section 3.2) and network fine-tuning (Section 3.3) steps, is currently set to 1 in SLR. Table 5 reports results with increasing the number of iterations. For reference, performance without the fine-tuning step is reported as well. Results show that a single fine-tuning step significantly boosts the performance compared to without using it, however, results do not improve with using further iterations. We thus conclude that a single fine-tuning step in SLR is sufficient.

#### 4.8 Comparison with label smoothing

The pseudo-label estimation step (Section 3.2) produces *soft* labels, which means that the distribution over labels at a given pixel is not collapsed to a single mode. We, therefore, tested the hypothesis that the observed improvements might actually come from the smoothed training labels, an effect reported in literature (Islam and Glocker, 2021).

We implemented a smoothing model that applies per-pixel and cross-pixel label smoothing

**Table 6** Ablation study on MODS (detection F1/F1<sub>D</sub>) and MaStr1325 validation set segmentation (mIoU<sub>tr</sub>). Enabling: static obstacle labels above the water edge ( $\mathbf{\hat{Y}}_{st}$ ), model fine-tuning (FT) from initial model predictions, applying constraints in fine-tuning (CO), feature-based label re-estimation (RE) and auxiliary warm-up loss  $\mathcal{L}_{aux}$ .

$\mathbf{\hat{Y}}_{st}$	FT	CO	RE	$\mathcal{L}_{aux}$	mIoU <sub>val</sub>	F1	F1 <sub>D</sub>
					97.4	87.7	54.9
✓					97.4	89.4 (+1.7)	71.0 (+16.1)
✓	✓				97.8	90.5 (+2.8)	84.9 (+30.0)
✓	✓	✓			98.2	93.0 (+5.3)	89.3 (+34.4)
✓	✓		✓		98.5	93.4 (+5.7)	89.7 (+34.8)
✓	✓	✓	✓		98.3	94.2 (+6.5)	91.4 (+36.5)
✓	✓	✓	✓	✓	<b>98.6</b>	<b>94.9</b> (+7.2)	<b>93.7</b> (+38.8)

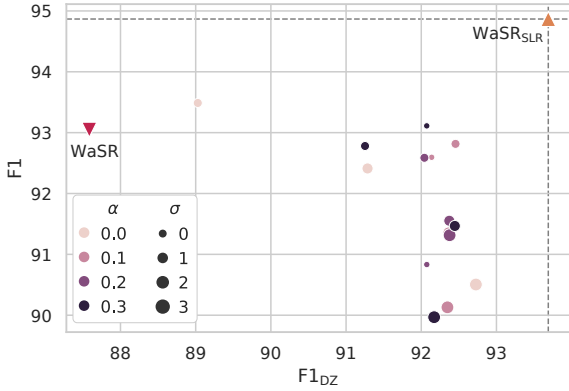


**Fig. 7** SLR pseudo-label estimation from weak annotations outperforms all combinations of spatial ( $\sigma$ ) and pixel-wise ( $\alpha$ ) label smoothing of dense GT in terms of overall and within danger zone obstacle detection F1 scores.

as follows. Let  $p_i$  be the label distribution at a pixel  $i$ . The new labels distribution is given as  $p'_i = p_i(1 - \alpha) + \frac{\alpha}{N}$ , where  $\alpha$  is the extent of smoothing and  $N$  is the number of label classes. The obtained label mask can be further spatially smoothed by a 2D Gaussian filter with size parameter  $\sigma$ . This model is applied to the one-hot ground truth segmentation labels in MaStr1325.

Results of exhaustive search over  $(\alpha, \sigma)$  are shown in Figure 7. As predicted by [Islam and Glocker \(2021\)](#), both types of label smoothing do improve the performance of the classically trained WaSR, particularly within the danger zone, albeit often at a slight overall performance decrease. Nevertheless, SLR training considerably outperforms all label smoothing combinations in both measures, despite using only weak annotations.

## 4.9 Qualitative analysis

Figure 8 visualizes the performance of WaSR and WaSR<sub>SLR</sub> on the MODS ([Bovcon et al, 2021](#)) dataset. Observe that SLR training reduces false-positive detections on wakes, sun glitter and reflections. Reduction of these is crucial for practical USV application since false positives result in frequent unnecessary slow-downs and effectively render the perception useless for autonomous navigation. Note that, while segmentation and thus obstacle detection substantially improves in regions important for navigation, structures such as masts are missed. However, these are in the areas irrelevant for navigation and not accounted for by supervision signals in SLR.

We next downloaded and captured several maritime photographs. These images were taken with various cameras, and we made sure they were out-of-distribution examples of scenes and vantage points not present in MaStr1325 ([Bovcon et al, 2019](#)). Since IMU data (horizon) is not available for these images, we re-trained WaSR<sub>SLR</sub> without IMU on MaStr1325. The results on the new images are shown in Figure 9.

A remarkable generalization to various conditions not present in the training data is observed. For example, WaSR<sub>SLR</sub> performs well even in night-time scenes, while only daytime images are present in MaStr1325. Furthermore, the training data contains only open, coastal sea cases, while high performance is obtained even in rivers and tight canals with different water colors and surface textures. We observe failure cases on thin structures (*e.g.*, part of surfboard missing) and false-positive detections on objects seen through

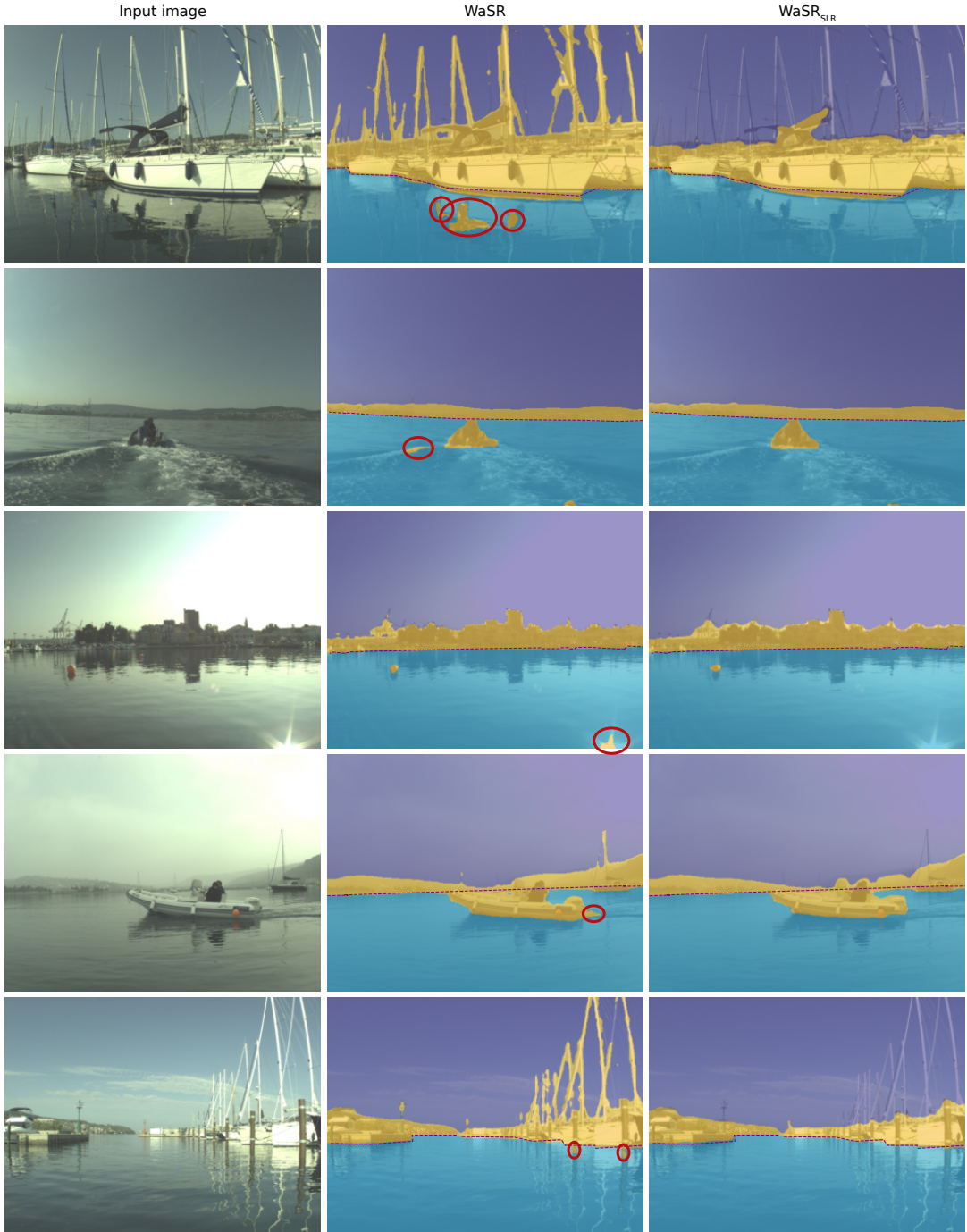


**Fig. 8** Comparison of WaSR and WaSR<sub>SLR</sub> on the MODS benchmark. WaSR<sub>SLR</sub> is less sensitive to false-positive detections on object reflections (rows 1 and 5), and performs well in challenging scenarios such as wakes (rows 2 and 4) and sun glitter (row 3).



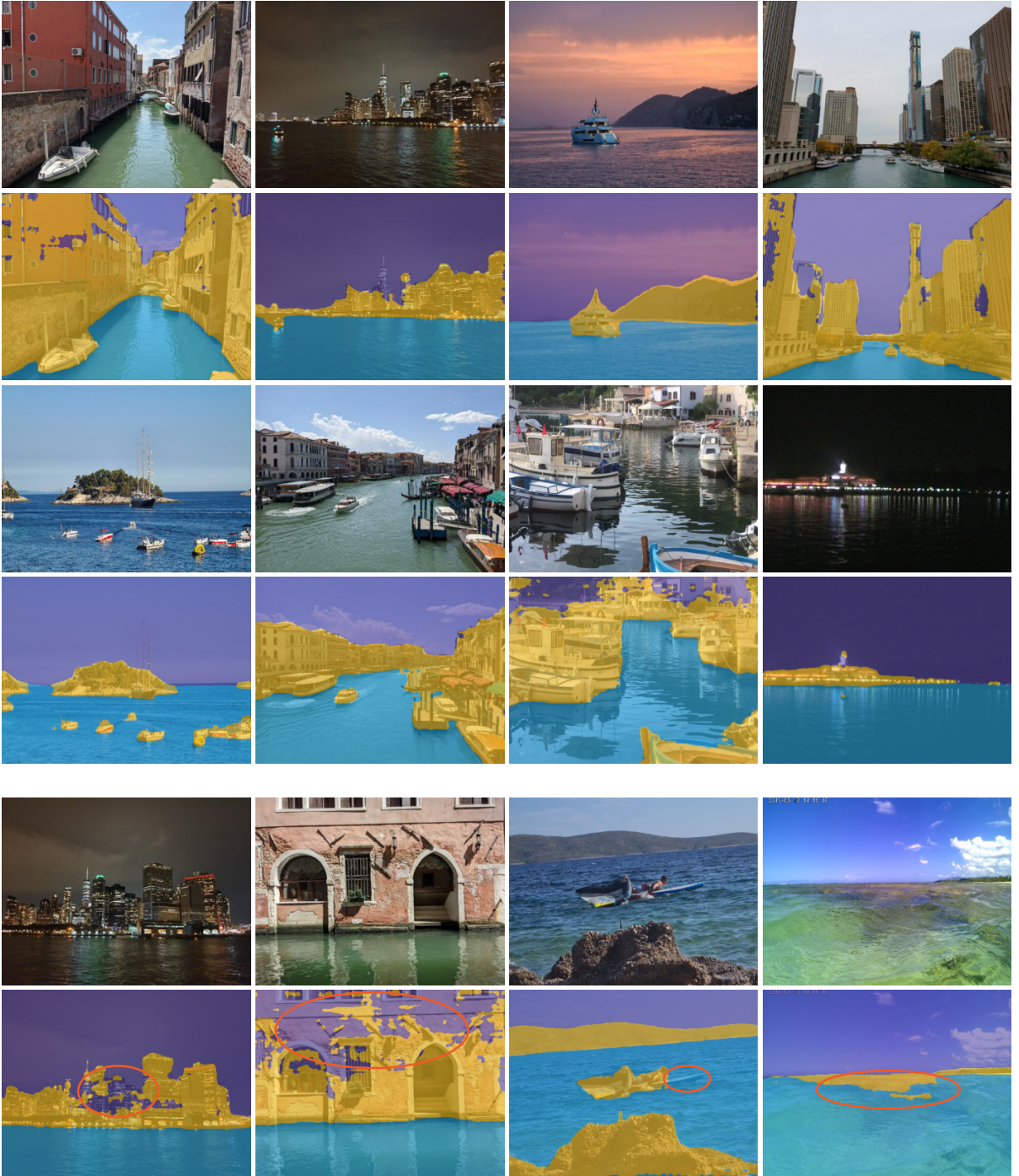


**Fig. 9** WaSR<sub>SLR</sub> performs surprisingly well in diverse maritime scenarios, including inland waters, different times of day and changes in water color. Failure cases are outlined in the last row and include sky hallucinations, partial detections of thin objects, and false detections of objects visible through the water.



shallow water. We also observe less accurate segmentation of top-most parts of static obstacles, which is not critical for obstacle detection, but indicates that further research could be invested in maritime segmentation networks to address such cases.

## 5 Conclusion

In this work, we proposed a novel scaffolding learning regime (SLR) for training maritime segmentation models for obstacle detection using only weak, detection-oriented, annotations. The main advantage of SLR is that it focuses only on aspects important for obstacle detection and significantly reduces the required labeling effort (by approximately 20 times). Models trained using SLR do not only match the performance of classically trained models, but outperform them by a large margin, setting a new state-of-the-art in segmentation-based maritime obstacle detection. Experiments indicate excellent domain generalization capabilities and a substantial potential in semi-supervised learning and domain adaptation. We also observed that SLR boost the performance of different network architectures.

In our future work, we plan to explore applications beyond the maritime domain such as autonomous cars and biomedical detection methods based on segmentation. Since SLR is complementary to semi-supervised learning methods such as (Huo et al, 2021), a combination or fusion of these approaches is another interesting research venue with a wide application spectrum.

**Acknowledgments.** This work was supported by the Slovenian Research Agency program P2-0214 and project J2-2506.

## References

Ahn J, Kwak S (2018) Learning Pixel-Level Semantic Affinity with Image-Level Supervision for Weakly Supervised Semantic Segmentation. In: Proceedings of the IEEE Computer Society Conference on Computer Vision and Pattern Recognition, <https://doi.org/10.1109/CVPR.2018.00523>

Akiva P, Dana K, Oudemans P, et al (2020) Finding berries: Segmentation and counting

of cranberries using point supervision and shape priors. In: IEEE Computer Society Conference on Computer Vision and Pattern Recognition Workshops, <https://doi.org/10.1109/CVPRW50498.2020.00033>

Bai X, Chen Z, Zhang Y, et al (2016) Infrared Ship Target Segmentation Based on Spatial Information Improved FCM. IEEE Transactions on Cybernetics 46(12):3259–3271. <https://doi.org/10.1109/TCYB.2015.2501848>

Bovcon B, Kristan M (2021) WaSR–A Water Segmentation and Refinement Maritime Obstacle Detection Network. IEEE Transactions on Cybernetics pp 1–14. <https://doi.org/10.1109/TCYB.2021.3085856>

Bovcon B, Muhovič J, Perš J, et al (2019) The MaStr1325 dataset for training deep USV obstacle detection models. In: 2019 IEEE/RSJ International Conference on Intelligent Robots and Systems (IROS), pp 3431–3438, <https://doi.org/10.1109/IROS40897.2019.8967909>

Bovcon B, Muhovič J, Vranac D, et al (2021) MODS – A USV-oriented object detection and obstacle segmentation benchmark. IEEE Transactions on Intelligent Transportation Systems

Cane T, Ferryman J (2019) Evaluating deep semantic segmentation networks for object detection in maritime surveillance. In: Proceedings of AVSS 2018 - 2018 15th IEEE International Conference on Advanced Video and Signal-Based Surveillance, <https://doi.org/10.1109/AVSS.2018.8639077>

Chan L, Hosseini MS, Plataniotis KN (2021) A Comprehensive Analysis of Weakly-Supervised Semantic Segmentation in Different Image Domains. International Journal of Computer Vision 129(2):361–384. <https://doi.org/10.1007/s11263-020-01373-4>

Chen LC, Papandreou G, Schroff F, et al (2017) Rethinking atrous convolution for semantic image segmentation. arXiv preprint arXiv:1706.05587 <https://arxiv.org/abs/arXiv:1706.05587>

- Chen LC, Papandreou G, Kokkinos I, et al (2018) DeepLab: Semantic Image Segmentation with Deep Convolutional Nets, Atrous Convolution, and Fully Connected CRFs. *IEEE Transactions on Pattern Analysis and Machine Intelligence* 40(4). <https://doi.org/10.1109/TPAMI.2017.2699184>
- Cheng Y, Jiang M, Zhu J, et al (2021) Are We Ready for Unmanned Surface Vehicles in Inland Waterways? The USVInland Multisensor Dataset and Benchmark. *IEEE Robotics and Automation Letters* 6(2):3964–3970
- Dai J, He K, Sun J (2015) BoxSup: Exploiting Bounding Boxes to Supervise Convolutional Networks for Semantic Segmentation. In: *Proceedings of the IEEE International Conference on Computer Vision (ICCV)*
- Durand T, Mordan T, Thome N, et al (2017) WILDCAT: Weakly Supervised Learning of Deep ConvNets for Image Classification, Point-wise Localization and Segmentation. In: *2017 IEEE Conference on Computer Vision and Pattern Recognition (CVPR)*. IEEE, Honolulu, HI, pp 5957–5966, <https://doi.org/10.1109/CVPR.2017.631>
- Hsu CC, Hsu KJ, Tsai CC, et al (2019) Weakly supervised instance segmentation using the bounding box tightness prior. In: *Advances in Neural Information Processing Systems*
- Hung WC, Tsai YH, Liou YT, et al (2019) Adversarial learning for semi-supervised semantic segmentation. In: *British Machine Vision Conference 2018, BMVC 2018*
- Huo X, Xie L, He J, et al (2021) ATSO: Asynchronous Teacher-Student Optimization for Semi-Supervised Image Segmentation. In: *Proceedings of the IEEE/CVF Conference on Computer Vision and Pattern Recognition (CVPR)*, pp 1235–1244
- Islam M, Glocker B (2021) Spatially Varying Label Smoothing: Capturing Uncertainty from Expert Annotations. In: *Information Processing in Medical Imaging*, pp 677–688, [2104.05788v1](https://doi.org/10.1007/s11263-019-01247-4)
- Kim H, Koo J, Kim D, et al (2019) Vision-Based Real-Time Obstacle Segmentation Algorithm for Autonomous Surface Vehicle. *IEEE Access* 7. <https://doi.org/10.1109/ACCESS.2019.2959312>
- Kristan M, Kenk VS, Kovačič S, et al (2016) Fast Image-Based Obstacle Detection from Unmanned Surface Vehicles. *IEEE Transactions on Cybernetics* 46(3). <https://doi.org/10.1109/TCYB.2015.2412251>
- Kulharia V, Chandra S, Agrawal A, et al (2020) Box2Seg: Attention Weighted Loss and Discriminative Feature Learning for Weakly Supervised Segmentation. In: *Lecture Notes in Computer Science (Including Subseries Lecture Notes in Artificial Intelligence and Lecture Notes in Bioinformatics)*, [https://doi.org/10.1007/978-3-030-58583-9\\_18](https://doi.org/10.1007/978-3-030-58583-9_18)
- Lee SJ, Roh MI, Lee HW, et al (2018) Image-based ship detection and classification for unmanned surface vehicle using real-time object detection neural networks. In: *Proceedings of the International Offshore and Polar Engineering Conference*
- Li Q, Arnab A, Torr PHS (2018) Weakly- and Semi-Supervised Panoptic Segmentation. In: *Proceedings of the European Conference on Computer Vision (ECCV)*, pp 102–118
- Lin G, Milan A, Shen C, et al (2017) RefineNet: Multi-path refinement networks for high-resolution semantic segmentation. In: *Proceedings - 30th IEEE Conference on Computer Vision and Pattern Recognition, CVPR 2017*, <https://doi.org/10.1109/CVPR.2017.549>
- Lin TY, Goyal P, Girshick R, et al (2020) Focal Loss for Dense Object Detection. *IEEE Transactions on Pattern Analysis and Machine Intelligence* 42(2). <https://doi.org/10.1109/TPAMI.2018.2858826>
- Liu L, Ouyang W, Wang X, et al (2020) Deep Learning for Generic Object Detection: A Survey. *International Journal of Computer Vision* 128(2):261–318. <https://doi.org/10.1007/s11263-019-01247-4>

- Ma L, Xie W, Huang H (2020) Convolutional neural network based obstacle detection for unmanned surface vehicle. *Mathematical Biosciences and Engineering* 17(1). <https://doi.org/10.3934/mbe.2020045>
- Maninis KK, Caelles S, Pont-Tuset J, et al (2018) Deep Extreme Cut: From Extreme Points to Object Segmentation. In: *Proceedings of the IEEE Computer Society Conference on Computer Vision and Pattern Recognition*, <https://doi.org/10.1109/CVPR.2018.00071>
- Mittal S, Tatarchenko M, Brox T (2019) Semi-Supervised Semantic Segmentation with High-And Low-Level Consistency. *IEEE Transactions on Pattern Analysis and Machine Intelligence* 43(4). <https://doi.org/10.1109/TPAMI.2019.2960224>
- Moosbauer S, Konig D, Jakel J, et al (2019) A benchmark for deep learning based object detection in maritime environments. In: *IEEE Computer Society Conference on Computer Vision and Pattern Recognition Workshops*, pp 916–925, <https://doi.org/10.1109/CVPRW.2019.00121>
- Pan J, Zhu P, Zhang K, et al (2022) Learning Self-supervised Low-Rank Network for Single-Stage Weakly and Semi-supervised Semantic Segmentation. *International Journal of Computer Vision* 130(5):1181–1195. <https://doi.org/10.1007/s11263-022-01590-z>
- Papandreou G, Chen LC, Murphy K, et al (2015) Weakly- and Semi-Supervised Learning of a DCNN for Semantic Image Segmentation. In: *Proceedings of the IEEE International Conference on Computer Vision (ICCV)*, 1502.02734
- Prasad DK, Rajan D, Rachmawati L, et al (2017) Video Processing From Electro-Optical Sensors for Object Detection and Tracking in a Maritime Environment: A Survey. *IEEE Transactions on Intelligent Transportation Systems* 18(8). <https://doi.org/10.1109/TITS.2016.2634580>
- Prasad DK, Prasath CK, Rajan D, et al (2019) Object Detection in a Maritime Environment: Performance Evaluation of Background Subtraction Methods. *IEEE Transactions on Intelligent Transportation Systems* 20(5):1787–1802. <https://doi.org/10.1109/TITS.2018.2836399>
- Qiao D, Liu G, Li W, et al (2022) Automated Full Scene Parsing for Marine ASVs Using Monocular Vision. *Journal of Intelligent & Robotic Systems* 104(2):1–20
- Ren S, He K, Girshick R, et al (2017) Faster R-CNN: Towards Real-Time Object Detection with Region Proposal Networks. *IEEE Transactions on Pattern Analysis and Machine Intelligence* 39(6):1137–1149. <https://doi.org/10.1109/TPAMI.2016.2577031>, <https://arxiv.org/abs/arXiv:1506.01497>
- Ronneberger O, Fischer P, Brox T (2015) U-net: Convolutional networks for biomedical image segmentation. In: *Lecture Notes in Computer Science (Including Subseries Lecture Notes in Artificial Intelligence and Lecture Notes in Bioinformatics)*, pp 234–241, [https://doi.org/10.1007/978-3-319-24574-4\\_28](https://doi.org/10.1007/978-3-319-24574-4_28), 1505.04597
- Steccanella L, Bloisi DD, Castellini A, et al (2020) Waterline and obstacle detection in images from low-cost autonomous boats for environmental monitoring. *Robotics and Autonomous Systems* 124. <https://doi.org/10.1016/j.robot.2019.103346>
- Tian Z, Shen C, Wang X, et al (2021) Box-Inst: High-Performance Instance Segmentation with Box Annotations. In: *Proceedings of the IEEE/CVF Conference on Computer Vision and Pattern Recognition*, pp 5443–5452, 2012. 02310
- Vernaza P, Chandraker M (2017) Learning random-walk label propagation for weakly-supervised semantic segmentation. In: *Proceedings - 30th IEEE Conference on Computer Vision and Pattern Recognition, CVPR 2017*, <https://doi.org/10.1109/CVPR.2017.315>
- Vu TH, Jain H, Bucher M, et al (2019) ADVENT: Adversarial Entropy Minimization for Domain Adaptation in Semantic Segmentation. In: *Proceedings of the IEEE/CVF Conference on Computer Vision and Pattern Recognition (CVPR)*,

1811.12833

- Wang H, Wei Z (2013) Stereovision based obstacle detection system for unmanned surface vehicle. In: 2013 IEEE International Conference on Robotics and Biomimetics, ROBIO 2013, <https://doi.org/10.1109/ROBIO.2013.6739579>
- Wang X, Liu S, Ma H, et al (2020a) Weakly-Supervised Semantic Segmentation by Iterative Affinity Learning. *International Journal of Computer Vision* 128(6):1736–1749. <https://doi.org/10.1007/s11263-020-01293-3>
- Wang X, Ma H, You S (2020b) Deep clustering for weakly-supervised semantic segmentation in autonomous driving scenes. *Neurocomputing* 381:20–28. <https://doi.org/10.1016/j.neucom.2019.11.019>
- Wang Y, Zhang J, Kan M, et al (2020c) Self-Supervised Equivariant Attention Mechanism for Weakly Supervised Semantic Segmentation. In: *Proceedings of the IEEE Computer Society Conference on Computer Vision and Pattern Recognition*, <https://doi.org/10.1109/CVPR42600.2020.01229>
- Yan B, Zhang X, Wang D, et al (2021) Alpha-Refine: Boosting Tracking Performance by Precise Bounding Box Estimation. In: *Proceedings of the IEEE/CVF Conference on Computer Vision and Pattern Recognition (CVPR)*, pp 5289–5298
- Yang J, Li Y, Zhang Q, et al (2019) Surface Vehicle Detection and Tracking with Deep Learning and Appearance Feature. In: 2019 5th International Conference on Control, Automation and Robotics, ICCAR 2019, <https://doi.org/10.1109/ICCAR.2019.8813345>
- Yang Y, Soatto S (2020) FDA: Fourier domain adaptation for semantic segmentation. In: *Proceedings of the IEEE Computer Society Conference on Computer Vision and Pattern Recognition*. IEEE Computer Society, pp 4084–4094, <https://doi.org/10.1109/CVPR42600.2020.00414>, 2004.05498
- Yao L, Kanoulas D, Ji Z, et al (2021) ShorelineNet: An Efficient Deep Learning Approach for Shoreline Semantic Segmentation for Unmanned Surface Vehicles. In: *Proceedings of the 2021 IEEE/RSJ International Conference on Intelligent Robots and Systems (IROS)*
- Yu C, Wang J, Peng C, et al (2018) BiSeNet: Bilateral segmentation network for real-time semantic segmentation. In: *Lecture Notes in Computer Science (Including Subseries Lecture Notes in Artificial Intelligence and Lecture Notes in Bioinformatics)*, pp 334–349, [https://doi.org/10.1007/978-3-030-01261-8\\_20](https://doi.org/10.1007/978-3-030-01261-8_20), 1808.00897
- Yu C, Gao C, Wang J, et al (2021) BiSeNet V2: Bilateral Network with Guided Aggregation for Real-Time Semantic Segmentation. *International Journal of Computer Vision* 129(11):3051–3068. <https://doi.org/10.1007/s11263-021-01515-2>
- Zhang J, Yu X, Li A, et al (2020a) Weakly-Supervised Salient Object Detection via Scribble Annotations. In: *Proceedings of the IEEE Computer Society Conference on Computer Vision and Pattern Recognition*, <https://doi.org/10.1109/CVPR42600.2020.01256>
- Zhang S, Liew JH, Wei Y, et al (2020b) Interactive Object Segmentation With Inside-Outside Guidance. In: *Proceedings of the IEEE/CVF Conference on Computer Vision and Pattern Recognition (CVPR)*
- Zhao B, Bhat G, Danelljan M, et al (2021) Generating Masks from Boxes by Mining Spatio-Temporal Consistencies in Videos. In: *IEEE/CVF International Conference on Computer Vision, ICCV*, 2101.02196
- Žust L, Kristan M (2022) Learning Maritime Obstacle Detection from Weak Annotations by Scaffolding. In: *Proceedings of the IEEE/CVF Winter Conference on Applications of Computer Vision*, pp 955–964, 2108.00564